International Journal of Fatigue 72 (2015) 75–79

Contents lists available at ScienceDirect

International Journal of Fatigue

journal homepage: www.elsevier.com/locate/ijfatigue

The role of microstructure in fatigue crack initiation of 9–12%Cr reduced activation ferritic–martensitic steel

M.N. Batista *, M.C. Marinelli, S. Hereñú, I. Alvarez-Armas

Instituto de Física Rosario, CONICET-UNR, Bv. 27 de Febrero 210 bis, 2000 Rosario, Argentina

ARTICLE INFO

Article history:
Received 9 September 2014
Received in revised form 6 November 2014
Accepted 10 November 2014
Available online 15 November 2014

Keywords:
Ferritic–martensitic steel
LCF
Microstructure
Microcrack nucleation
EBSD technique

ABSTRACT

Electron back-scattered diffraction together with scanning and transmission electron microscopy were used to study nucleation of microstructural fatigue cracks in reduced-activation ferritic–martensitic steel, EUROFER 97. Cylindrical specimens were cycled over different plastic-strain ranges in order to evaluate the evolution of the dislocation structure. Surface-damage evolution was studied in smooth notched specimens by an optical *in situ* system equipped with a high-resolution camera. In order to understand the crack-initiation mechanism, the dislocation microstructure that develops in the near-surface regions of the notch was compared with that of the bulk. The results demonstrate a strong influence of lath-martensite boundaries on fatigue-crack nucleation.

1. Introduction

Microcrack initiation, microcrack growth and coalescence and final failure comprise damage accumulation under fatigue loading. The microstructure and mechanical properties of the materials strongly affect crack initiation and its subsequent propagation. Small cracks nucleate mainly at the surface in higher plastic-strain concentration areas. Slip bands, inclusions, grain boundaries, and twin boundaries can produce local plastic-strain concentrations [1]. The formation of persistent slip bands (PSBs) [2] is a well-known small-crack initiation mechanism. In areas where PSBs intersect the surface, extrusions and intrusions, surface relief features, arise leading to fatigue crack nucleation [3]. Recently, Polak and Man proposed a mechanism which explains the formation of extrusions and especially of intrusions based on the plastic relaxation of internal compression stresses in PSBs and internal tensile stresses in the matrix [4].

The nuclear industry uses 9–12%Cr ferritic–martensitic steels and in particular reduced-activation, ferritic–martensitic (RAFM) steels with 9%Cr due to their excellent thermal properties and swelling resistance [5]. Frequently, normalized and tempered thermal treatments are carried out on these steels in order to increase toughness and ductility [6]. In the normalized condition, martensite laths contain a high dislocation density [7]. When tempered, the dislocation structure recovers and the former martensite lath develops into elongated subgrains, typically with an average width of 0.25–0.5 μm. Depending on the tempering conditions, laths contained within the prior-austenite grain boundaries have a relatively high dislocation density (10^{13}–10^{14} m^2). Additionally, $M_{23}C_6$ precipitates are observed, mainly on lath boundaries and prior-austenite grain boundaries causing pinning effects [7,8]. It is evident that in these kinds of steel, with a pre-established microstructure, the process of fatigue damage and in particular of microcrack initiation may not follow the steps widely reported in the literature for other alloys. That is the development of a characteristic dislocation structure followed by the process of strain localization and further extrusion formation.

Previous low-cycle fatigue studies on 9–12%Cr ferritic–martensitic steels attributed the cyclic softening, which occurs over a wide range of strains and temperatures, to the microstructural instability of the high initial dislocation density [9–15]. Nowadays, the softening stage in 9–12%Cr steels and especially in RAFM steels is clearly associated with the increase of the subgrain size, regardless of the temperature [13]. Moreover, the softening has been at least partially explained by annihilation of dislocations within subgrains [12] and by lath/sub-grain boundary elimination [16].

Although cyclic softening has been extensively studied in the literature, evidence of a strain concentration structure or structures associated with crack nucleation is very scarce. Kruml et al. [17] have studied the low-cycle fatigue (LCF) behavior at room temperature of two high-chromium, 14%Cr, ferritic steels, which are still under development for the future fusion reactor. These steels have ultrafine grains and fine oxide dispersion

* Corresponding author. Tel./fax: +54 341 4853200.
E-mail address: batista@ifir-conicet.gov.ar (M.N. Batista).

http://dx.doi.org/10.1016/j.ijfatigue.2014.11.006
0142-1123/

Table 1
Chemical composition in weight percent of EUROFER 97.

C	N	Si	Mn	Ni	Cr	Mo	W	V	Ta	Nb	Al	Ti	Cu	Fe
0.12	0.018	0.06	0.47	0.022	8.93	0.0015	1.07	0.2	0.14	–	0.008	0.01	0.004	Bal.

Table 2
Heat treatments of the steels: normalization/air cooling and tempering/air cooling.

Steels	Normalization	Tempering
EUROFER 97	980 °C/0.5 h	760 °C/1.5 h

strengthening. These authors do not discuss the formation of extrusions and intrusions due to cyclic straining. However, they have observed that nucleation and early growth of fatigue cracks are enhanced by the surface relief.

This paper analyzes the effect of the initial tempered-lath microstructure on the surface relief and crack initiation developed during cyclic straining of a RAFM EUROFER 97 steel.

2. Experimental procedure

The material considered in this study was the reduced activation ferritic–martensitic steel EUROFER 97 with a chemical composition shown in weight percent in Table 1. Before testing, the steel was normalized and tempered according to the schedule in Table 2 (after each heat treatment the steel was air cooled).

The steel has a tempered martensitic-lath microstructure, Fig. 1a, composed of small, 0.5 μm average diameter, subgrains with an appreciable dislocation density in their interiors, Fig. 1b. $M_{23}C_6$ carbides, about 60–150 nm in diameter, were distributed preferentially along lath boundaries and prior-austenite grain boundaries, forming rows of precipitates. Fig. 1c shows the superimposed Inverse Pole Figure and Image Quality maps (IPF + IQ-map) of an EBSD-scan of the as-received material. From this figure a statistical map of the lath and subgrain structure of the as-received EUROFER 97 can be obtained. The micrograph shows two contrasting structures: (i) small, highly misoriented areas and (ii) large, slightly misoriented areas.

In order to correlate the cyclic behavior of the steel and the dislocation structure it develops during cycling, low-cycle fatigue

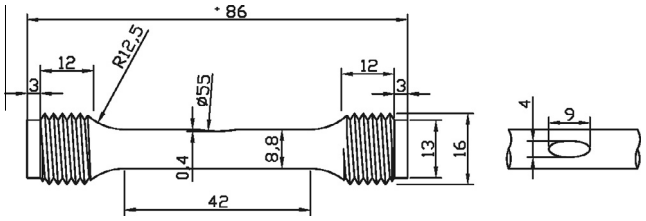

Fig. 2. Diagram of the shallow-notched specimen.

tests were performed on solid specimens with a cylindrical gauge section. The samples were 77 mm long and 8.8 mm in diameter. The tests were performed in plastic-strain control using a triangular wave over a strain range of $\Delta\varepsilon_p = 0.2\%$, 0.3% and 0.6% with a total strain rate of $\dot{\varepsilon} = 3 \times 10^{-3}\ s^{-1}$. Additionally, studies of microcrack initiation and growth during fatigue were carried out on very shallow notched cylindrical specimens over a strain range of $\Delta\varepsilon_p = 0.2\%$, Fig. 2. The notch focuses the fatigue damage in an observation zone, with a stress concentration factor of 1.06 at the notch tip. The surface of the shallow notch was mechanically and electrolytically polished to improve the observation of microcrack nucleation and growth. The central part of the notch was monitored during the test using a powerful *in situ* optical system consisting of a CCD camera, JAI model CM-140MCL with a 50X objective, ±1 μm FD and 13 mm WD and a 12× ultra zoom. After 300 cycles the specimens were removed from the testing machine and the shallow-notch areas examined with high-resolution scanning electron microscopy (SEM-FEG). In addition, the surface was scanned by EBSD to get crystallographic data from the tempered structure associated with surface damage.

The dislocation structure in the bulk of the cylindrical specimen was observed by cutting transverse disks from the gauge section and near the surface by taking slices at different depths from the

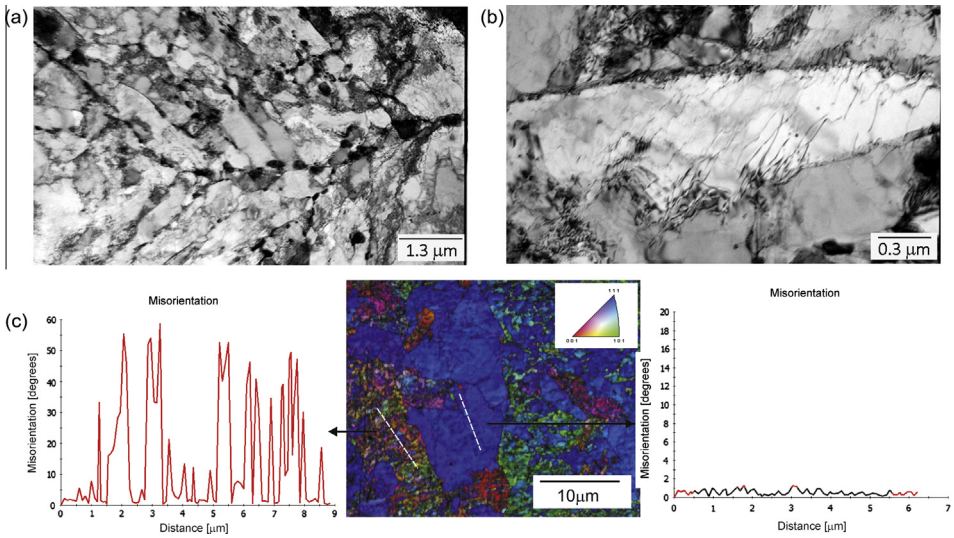

Fig. 1. Microstructure of EUROFER 97: (a) a general TEM view of the as-received material; (b) a detailed image of a subgrain from which the lath structure is composed; (c) IPF [001] + IQ map showing areas with a very fine and disoriented subgrain structure (left) and other areas composed of larger subgrains with slight misorientations (right).

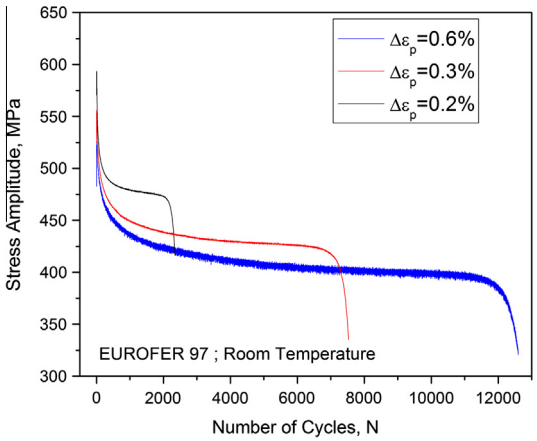

Fig. 3. Cyclic deformation behavior of EUROFER 97 for different plastic-strain ranges.

shallow-notched area parallel to the specimen axis. Thin foils were prepared by double-jet thinning using a solution of 10% perchloric acid and ethanol, keeping the current density and temperature at 60 mA and −15 °C, respectively. Observations of dislocation structures were performed using a Transmission Electron Microscope (TEM) operated at 100 kV to analyze the evolution of the dislocation structure.

3. Results and discussion

The cyclic behavior of EUROFER 97 at room temperature under plastic-strain control for different strain ranges is shown in Fig. 3. Independently of the imposed strain range, after the first few cycles, the steel shows a cyclic softening that continues up to failure.

Although Jones and Fernández Paredes have demonstrated the stability of a normalized and tempered microstructure for a 9–12%Cr modified ferritic–martensitic steel during subsequent annealing [18,5], the tempered lath structure is strongly unstable under cyclic conditions. The laths are gradually replaced by the development of a subgrain structure [9,15,19]. Minimizing their stored energy, the original parallel high dislocation-density martensitic laths partition into an equiaxed subgrain structure of large diameter, the exact dimensions of the subgrains depends on the applied plastic-strain range. In the bulk of the specimen, dislocation-free areas are frequently observed in regions near the lath boundaries. These areas are larger at large plastic strain, Fig. 4a and c. In particular, Fig. 4b and d details the two extreme strain ranges of the dislocation annihilation and rearrangement that leads to the low-angle subgrain structure. In fact, the lath interiors are nearly free of dislocations and the subgrain walls are well-defined. It is important to remark that dislocation stress concentrators like pile-ups or arrangements impinging at boundaries are rarely observed in the bulk of the cycled specimen. Nevertheless, observations in the near-surface regions are characterized not only by low-energy stable structures, like those observed in the bulk, but also by arrangements of dislocations generating stress concentrations at lath boundaries, Fig. 4e and f. Moreover, the dislocation activity within subgrains is more pronounced and dislocation pile-ups of different lengths are frequently observed. In fact, pile-up length depends on subgrain size. It is interesting that the subgrain size near the surface in the area of the notch is on average smaller than in the bulk. In the bulk, the average subgrain diameter is about 1.1 μm, while near the surface areas this value decreases to an average of 0.3 μm.

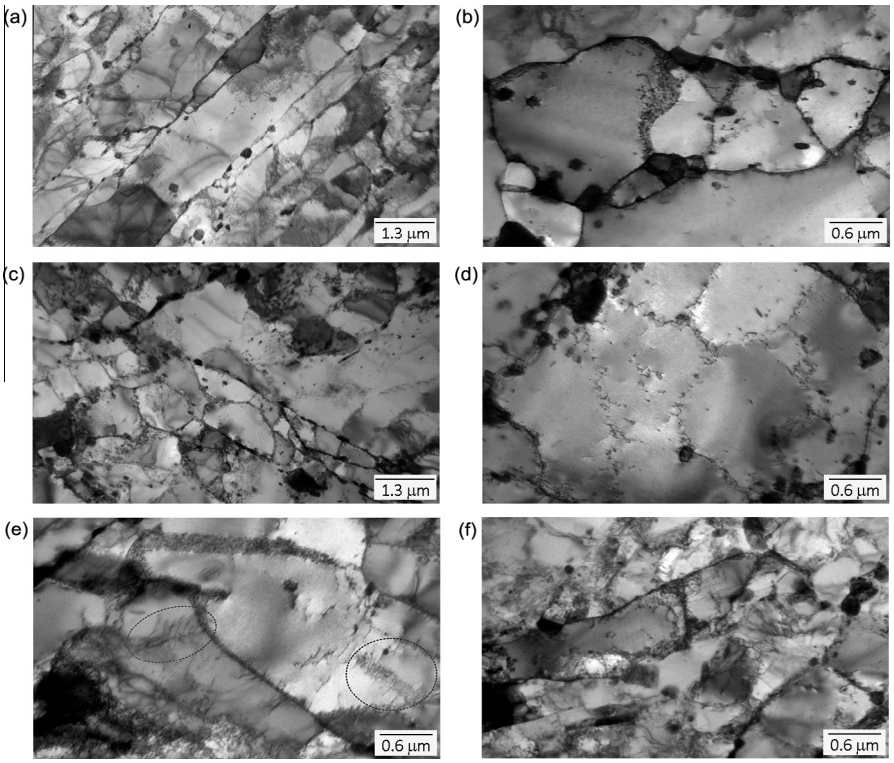

Fig. 4. (a) $\Delta\varepsilon_p = 0.2\%$: the original parallel martensitic laths are partitioned into equiaxed subgrains of larger diameter; (b) detail of the cell structure; (c) general structure developed at $\Delta\varepsilon_p = 0.6\%$; (d) detail of the cell structure $\Delta\varepsilon_p = 0.6\%$. Zones of high localized stresses at lath and subgrain boundaries have developed near the surface of the notched specimen cycled at $\Delta\varepsilon_p = 0.2\%$ (e) and (f).

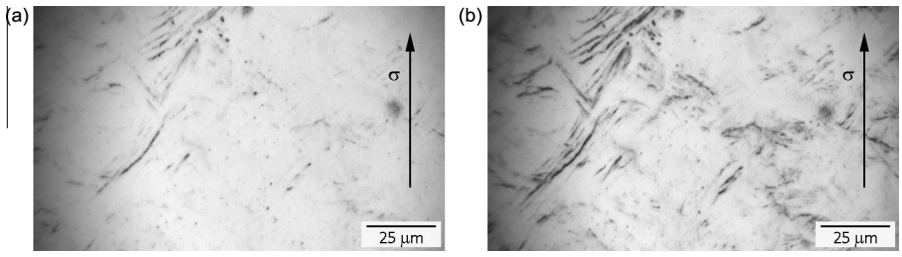

Fig. 5. *In situ* micrographs of surface damage seen in EUROFER 97. The observations were made during fatigue tests at: (a) 100 cycles; (b) 300 cycles.

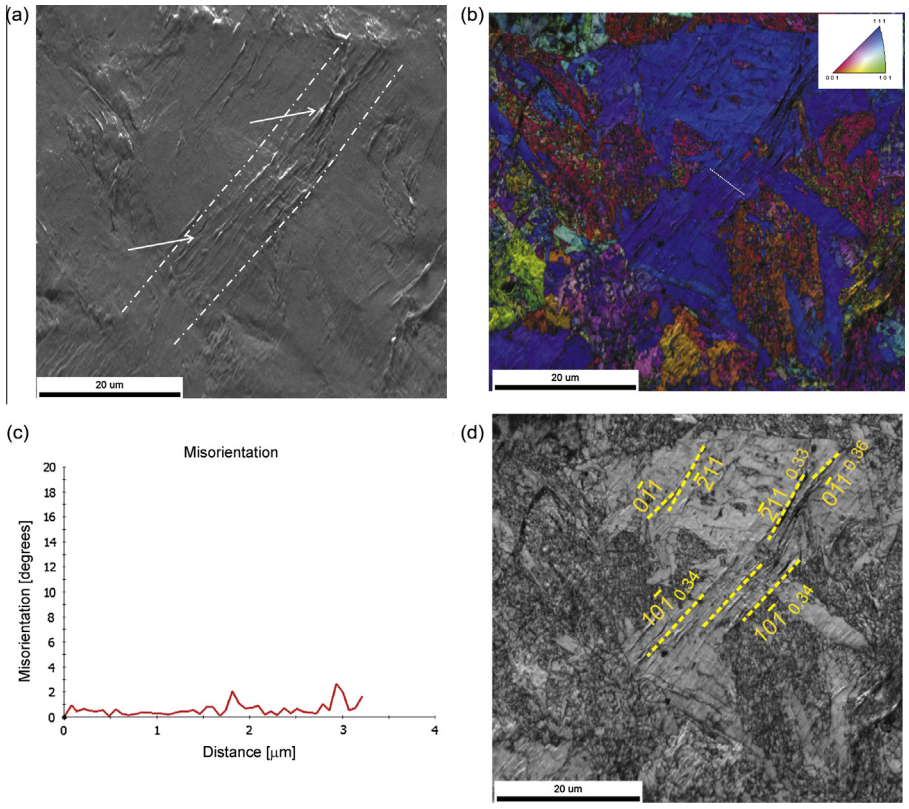

Fig. 6. Surface damage of EUROFER 97 observed by SEM-EBSD maps: (a) secondary electron image; (b) IPF [0 0 1] + IQ map and (c) distribution of local misorientation along a line crossing a rough area; (d) IQ maps showing activated slip planes and associated Schmid factors.

The *in situ* observations during LCF show that before completion of 100 cycles the first deformation lines appear along lath boundaries oriented at about 45° with respect to the tensile axis, Fig. 5a. After a certain number of cycles, these lines intensify and turn into slip bands forming a rough surface, from which, finally, the microcracks nucleate, Fig. 5b. These results were corroborated by high resolution SEM observations. During cycling, microcrack nucleation along lath boundaries has already been reported in another type of 9–12%Cr ferritic–martensitic steel [20].

Fig. 6 shows the surface topography of the tempered lath-martensite structure developed during a low-cycle fatigue test at $\Delta\varepsilon_p = 0.2\%$. The observations after 300 cycles were made by: (a) SEM-secondary electrons; (b) superimposed Inverse Pole and Image Quality maps (IP + IQ-map) from an EBSD-scan and (c) IQ map showing the topography, activated slip planes and Schmid factors. The SEM image, Fig. 6a, shows the intrusions/extrusions in the area between the dashed lines, and the nucleation of some microcracks originating from the surface relief (marked by arrows). Meanwhile, Fig. 6b shows the IP + IQ map of the same area. It is clear that the surface relief (intrusions/extrusions) is formed over a large area of slightly misoriented lath structures. The misorientation profile is plotted in Fig 6d from a slightly rough area of Fig. 6b. According to Fig. 6c, the misorientation between neighboring laths is about 0.8° on average and there is a pronounced peak associated with overcoming an extrusion. Fig. 6d shows the activated slip planes in the slighted misoriented area, corresponding to {1 1 0} and {1 1 2} families with a Schmid factor higher than 0.3. At least at this scale, the areas with a definite lath and subgrain structure do not seem to be affected by cyclic deformation.

This result is surprising when it is compared to the work of Kruml et al. [17], who were working with 14%Cr ferritic steels. These authors do not report the development of extrusions/intrusions associated with a dislocation structure for subgrain size less than 1 μm. They explain this based on an incompatibility of the characteristic dimensions of such structures with the subgrain size.

TEM results document the different dislocation behaviors whether the observations are taken from the near-surface regions of the notch, where the strain is highly concentrated, or from the bulk of the specimen, in which case the strain is homogeneously distributed over the whole gauge length. It is evident that the near-surface region has been hardened preferentially due to a smaller subgrain size. Consequently, a combination of the high

mechanical stresses and the absence of strain constraint normal to the surface ease the initiation of microplasticity at the surface. As well, the existence of dislocation stress concentrations like pile-ups speaks to the irreversibility of slip during cycling straining. Irreversible slip is in fact much more pronounced in the near-surface regions than in the bulk. According to Mughrabi [21] local accumulation of dipole pile-ups caused by this irreversibility is the origin of crack initiation. Additionally, Tanaka and Mura [22] proposed a model predicting crack initiation, based on the assumption that dislocation dipole effects on slip bands increase the stored energy in a stepwise manner until a critical value is reached after a defined number of cycles. In their work, Brückner-Foit and Huang [23] used this relation to simulate damage accumulation by continuous crack initiation in another grade of RAFM steel. They concluded that the overall process of damage accumulation is well described by the Tanaka–Mura model.

4. Conclusions

In the ferritic–martensitic steel EUROFER 97 studied here, the correlation between microstructural evolution and microcrack nucleation showed that lath boundaries are favorable sites for microcrack nucleation. This result can be understood in terms of irreversible, cyclic strain due to the formation of pile-ups occurring preferentially near the surface.

Acknowledgements

This work was supported by Consejo Nacional de Investigaciones Científicas y Técnicas – Argentina (CONICET).

References

[1] Suresh S. Fatigue of materials. 2nd ed. Cambridge University Press; 1998.
[2] Polak J. Cyclic plasticity and low cycle fatigue life of metals. Amsterdam: Elsevier; 1991.
[3] Man J, Obrtlik K, Polak J. Extrusions and intrusions in fatigued metals. Part 1. State of the art and history. Philos Mag 2009;89:1295–336.
[4] Polak J, Man J. Mechanisms of extrusion and intrusion formation in fatigued crystalline materials. Mater Sci Eng A 2014;596:15–24.
[5] Fernández Paredes M, Estudio de las propiedades metalúrgicas de los aceros martensíticos de activación reducida para su aplicación en los reactores de fusión. PhD Thesis. Universidad Carlos III, Madrid; 2007. <http://hdl.handle.net/10016/2369>.
[6] Jitsukawa S, Tamura M, van der Schaaf B, Klueh RL, Alamo A, Petersen C, et al. Development of an extensive database of mechanical and physical properties for reduced-activation martensitic steel F82H. J Nucl Mater 2002;307–311:179–86.
[7] Klueh RL, Nelson AT. Ferritic–martensitic steels for next-generation reactors. J Nucl Mater 2007;371:37–52.
[8] Zeman A, Debarberis L, Kocik J, Slugen V, Keilová E. Microstructural analysis of candidate steels pre-selected for new advanced reactor systems. J Nucl Mater 2007;362:259–67.
[9] Armas AF, Petersen C, Schmitt R, Avalos M, Alvarez I. Cyclic instability of martensite laths in reduced activation ferritic–martensitic steels. J Nucl Mater 2004;329–333:252–6.
[10] Giordana MF, Giroux P-F, Alvarez-Armas I, Sauzay M, Armas AF, Kruml T. Microstructure evolution during cyclic tests on EUROFER 97 at 20 C: TEM observation and modeling. Mater Sci Eng A 2012;550:103–11.
[11] Giordana MF, Alvarez-Armas I, Armas AF. Microstructural characterization of EUROFER 97 during LCF. J Nucl Mater 2012;424:247–51.
[12] Giordana MF, Alvarez-Armas I, Armas A. On the cyclic softening mechanisms of reduced activity ferritic–martensitic Steels. Steel Res Int 2012;83(6):594–9.
[13] Marmy P, Kruml T. Low cycle fatigue of EUROFER 97. J Nucl Mater 2008;377:52–8.
[14] Saad AA, Sun W, Hyde TH, Tanner DWJ. Cyclic softening behavior of a P91 steel under LCF high temperature. Procedia Eng 2011;10:1103–8.
[15] Kim DW, Kim SS. Contribution of microstructure and slip system to cyclic softening of 9 wt.% Cr steel. Int J Fatigue 2012;36:24–9.
[16] Sauzay M, Brillet H, Monnet I, Mottot M, Barcelo F, Fournier B, et al. Mater Sci Eng A 2005;400–401:241–4.
[17] Kruml T, Kubena I, Polak J. Fatigue behaviour and surface relief in ODS steels. Procedia Eng 2011;10:1685–90.
[18] Jones W, Hills CR, Polonis DH. Microstructural evolution of modified 9Cr–1Mo steel. Metall Trans 1991;22A:1049–58.
[19] Fournier B, Sauzay M, Renault A, Barcelo F, Pineau A. Microstructural evolutions and cyclic softening of 9%Cr martensitic steels. J Nucl Mater 2009;386–388:71–4.
[20] Batista MN, Hereñú S, Alvarez-Armas I. The role of microstructure in fatigue crack initiation and propagation in 9–12Cr ferritic–martensitic steels. Procedia Eng 2014;74:228–31.
[21] Mughrabi H. Cyclic slip irreversibilities and the evolution of fatigue damage. Metall Mater Trans A 2009;40:1257–79.
[22] Tanaka K, Mura T. A dislocation model for fatigue crack initiation. J Appl Mech 1981;48:97–103.
[23] Brückner-Foit A, Huang X. Numerical simulation of micro-crack initiation of martensitic steel under fatigue loading. Int J Fatigue 2006;28:963–71.